Since January 2020 Elsevier has created a COVID-19 resource centre with free information in English and Mandarin on the novel coronavirus COVID-19. The COVID-19 resource centre is hosted on Elsevier Connect, the company's public news and information website.

Pharmacological Research 157 (2020) 104820

Contents lists available at ScienceDirect

Pharmacological Research

journal homepage: www.elsevier.com/locate/yphrs

Chemical composition and pharmacological mechanism of Qingfei Paidu Decoction and Ma Xing Shi Gan Decoction against Coronavirus Disease 2019 (COVID-19): *In silico* and experimental study

Ruocong Yang[a,1], Hao Liu[b,1], Chen Bai[a,1], Yingchao Wang[b], Xiaohui Zhang[b], Rui Guo[b], Siying Wu[a], Jianxun Wang[a], Elaine Leung[c], Hang Chang[d], Peng Li[a], Tiegang Liu[a,*], Yi Wang[b,*]

[a] School of Traditional Chinese Medicine, Beijing University of Chinese Medicine, Bei San Huan East Road, Beijing, 100029, China
[b] Pharmaceutical Informatics Institute, College of Pharmaceutical Sciences, Zhejiang University, Hangzhou, 310058, China
[c] Macau University of Science & Technology, Macau, China
[d] Lawrence Berkeley National Laboratory, University of California, USA

ARTICLE INFO

Chemical compounds studied in this article:
Amygdalin (PubChem CID: 656516)
Baicalin (PubChem CID: 64982)
Ephedrine (PubChem CID: 9294)
Glycyrrhizic acid (PubChem CID: 14982)
Hesperidin (PubChem CID: 10621)
Narirutin (PubChem CID: 442431)
Neohesperidin (PubChem CID: 442439)

Keywords:
Qingfei Paidu Decoction
Ma Xing Shi Gan Decoction
Corona virus disease 2019
Network pharmacology
Traditional Chinese medicine

ABSTRACT

The Coronavirus Disease 2019 (COVID-19) pandemic has become a huge threaten to global health, which raise urgent demand of developing efficient therapeutic strategy. The aim of the present study is to dissect the chemical composition and the pharmacological mechanism of Qingfei Paidu Decoction (QFPD), a clinically used Chinese medicine for treating COVID-19 patients in China. Through comprehensive analysis by liquid chromatography coupled with high resolution mass spectrometry (MS), a total of 129 compounds of QFPD were putatively identified. We also constructed molecular networking of mass spectrometry data to classify these compounds into 14 main clusters, in which exhibited specific patterns of flavonoids (45 %), glycosides (15 %), carboxylic acids (10 %), and saponins (5 %). The target network model of QFPD, established by predicting and collecting the targets of identified compounds, indicated a pivotal role of Ma Xing Shi Gan Decoction (MXSG) in the therapeutic efficacy of QFPD. Supportively, through transcriptomic analysis of gene expression after MXSG administration in rat model of LPS-induced pneumonia, the thrombin and Toll-like receptor (TLR) signaling pathway were suggested to be essential pathways for MXSG mediated anti-inflammatory effects. Besides, changes in content of major compounds in MXSG during decoction were found by the chemical analysis. We also validate that one major compound in MXSG, i.e. glycyrrhizic acid, inhibited TLR agonists induced IL-6 production in macrophage. In conclusion, the integration of *in silico* and experimental results indicated that the therapeutic effects of QFPD against COVID-19 may be attributed to the anti-inflammatory effects of MXSG, which supports the rationality of the compatibility of TCM.

1. Introduction

Coronavirus Disease 2019 (COVID-19), which is caused by the novel coronavirus acute respiratory syndrome coronavirus type 2 (SARS-CoV-2), has become a serious threaten for public health worldwide [1]. This novel coronavirus has relatively fast transmission speed, which make COVID-19 a highly contagious disease [2,3]. As of March 26, 2020, the epidemic has been sweeping through over 100 countries or regions, and the pandemic has spread to all continents except Antarctica [4], and a total of 531,630 people worldwide were infected with the virus, of whom 24,065 died [5].

Cytokine storm is considered to be one of the leading causes of the clinical deterioration of COVID-19. Through laboratory blood cell counts, lymphopenia was detected in 83.2 % of the patients upon admission, the proportion of which was higher in those with severe illness than non-severe cases [6]. Meanwhile, 36.2 % of patients had thrombocytopenia, and 33.7 % of patients had leukopenia [6]. The reduction of white blood cells and platelets in the bloodstream may be a result of the over-mobilization and aggregation of immune cells in the lesion area for inflammation control. The occurrence of immune cells detachment from blood vessels increases the risk of excessive immune response and directly leads to cytokine storms [7]. When a large number of immune cells are concentrated in the lesion area, a great amount of cytokines are secreted through positive feedback stimulation

* Corresponding authors.
E-mail addresses: liutg@bucm.edu.cn (T. Liu), zjuwangyi@zju.edu.cn (Y. Wang).
[1] Ruocong Yang, Hao Liu and Chen Bai have equal contributions to this study.

https://doi.org/10.1016/j.phrs.2020.104820
Received 29 March 2020; Received in revised form 5 April 2020; Accepted 7 April 2020
Available online 29 April 2020

between each other. Consequently, the immune cells will be activated excessively, which cause tissue damage in the lesion area, as well as severe immune overreaction in the body. This pathological process may directly leads to hypoxemia, shock, and multiple organs failure [8]. Therefore, reducing the excessive aggregation and response of immune cells is important for the prevention of cytokine storms and is beneficial for patient outcomes.

According to a World Health Organization (WHO) commentary, there are currently no effective drugs for the treatment of COVID-19 [9], and the four most promising coronavirus treatments are still undergoing clinical trials [10]. Moreover, for controlling cytokine storms, only hormones and artificial liver blood purification systems are available at present [11]. However, the use of glucocorticoids cannot alleviate the progression of lung injury during COVID-19 infection, yet the side effects of glucocorticoids may significantly reduce life quality of patients [12,13]. Meanwhile, the application of artificial liver blood purification systems also faces challenges as this technology has not been widely used in clinical. Therefore, the successful treatment of COVID-19 patients, especially those severe cases with severe cytokine storms, were impeded.

Since the outbreak of COVID-19, traditional Chinese medicine (TCM) has been used as first-line drugs to treat patients in China and has obtained positive curative effects. As of February 22, 2020, the rate of TCM treatment of COVID-19 in China was 87 %, and the total effective rate of TCM treatment was 92 %, of which only 5% of patients have worsened clinical manifestations [14–16]. The Chinese government decided TCM as one of the recommended therapeutic options for the treatment of COVID-19 in the third version *COVID-19 treatment guidelines*, which was published on January 23, 2020 [17]. Besides, based on the theoretical system of TCM, physicians can combine and adjust prescriptions based on the symptoms of patients diagnosed. After nearly one month of clinical experimental observation, Qingfei Paidu Decoction, a formula consisting of 21 components including both herbs and mineral drugs, has been included in the 6th edition of the guidelines as the primarily recommended formulae [18]. According to the 6th and 7th edition of *COVID-19 treatment guidelines* [19,20], Qingfei Paidu Decoction (QFPD) is effective for patients at all stages, and the total effective rate is 92.09 % [21]. However, whether QFPD treat COVID-19 through regulating immune status and preventing cytokine storms has not been fully elucidated.

Here, we integrated multidisciplinary technologies to explore the pharmacological mechanism and to identify the major constituents of QFPD. The chemical constituents in QFPD was dissected by liquid chromatograph-mass spectrometry (LC–MS), and a substance-based intervention network was established through network pharmacology. At the same time, a disease network of patients based on their description of TCM symptoms was built via the SymMap database. Then, through network analysis, we analyzed the regulating pathways of QFPD and conducted biological verification via an *in vitro* macrophage activation model. Moreover, the chemical composition and pharmacological effects of a main component of Qingfei Paidu Decoction, Ma Xing Shi Gan Decoction, was further verified by transcriptomics. In summary, our study demonstrated Qingfei Paidu Decoction regulates the level of cytokine storms during the infection, which may be key mechanism underlying its therapeutic effects in COVID-19. These results may also guide future researches on TCM in infectious diseases and hyperimmune-related diseases.

2. Experimental

2.1. Materials and reagents

The reference compounds wogonin, cryptochlorogenic acid, neochlorogenic acid, chlorogenic acid, rosmarinic acid, mangiferin, irisflorentin, amygdalin, baicalin, iristectorin, 3,4-dicaffeoylquinic acid, 3,5-dicaffeoylquinic acid, rutin, naringin, narirutin, neohesperidin, hesperidin, isoacteoside, saikosaponin B2, saikosaponin A, wogonoside were purchased from Shanghai Winherb Medical Technology Co., Ltd (Shanghai, China). Quercetin, isoliquiritin, isoliquiritin apioside, acteoside, 25-O-methylalisol A, alisol C monoacetate, glycyrrhizic acid were purchased from Shanghai Yuanye Bio-Technology Co., Ltd (Shanghai, China). Quercitrin was were obtained from Aladdin Industrial Corporation (Shanghai, China). Ephedrine and pseudoephedrine were from National Institutes for Food and Drug Control (Beijing, China). HPLC-grade acetonitrile, methanol and formic acid were from Merk (Darmstadt, Germany). Deionized water was prepared with an Elga PURELAB flex system (ELGA LabWater, UK). All other chemicals and reagents used were of analytical grade. The crude drug materials were obtained from China Beijing Tongrentang (Group) Co., Ltd. High-glucose Dulbecco's modified Eagle's medium, fetal bovine serum, trypsin-EDTA and antibiotics (100 U/mL penicillin G and 100 g/mL streptomycin) were obtained from Gibco BRL (Grand Island, NY, USA). Poly(I:C) and Pam3CSK4 were purchased from InvivoGen (Carlsbad, CA, USA). IL-6 ELISA kit was obtained from Boster Biological Technology Co., Ltd (Wuhan, China).

2.2. Sample preparation

Qingfei Paidu Decoction was prepared from 21 herbs, *Herba Ephedrae* (Ma Huang), *Radix Glycyrrhizae* (Gan Cao, baked), *Semen armeniacae amarum* (Ku Xing Ren), *Gypsum fibrosum* (Sheng Shi Gao), *Ramulus Cinmomi* (Gui Zhi), *Rhizoma Alismatis* (Ze Xie), *Polyporus umbellatus* (Zhu Ling), *Atractylodis Macrocephalae Rhizoma* (Bai Zhu), *Poria* (Fu Ling), *Stellariae Radix* (Chai Hu), *Radix Scutellariae* (Huang Qin), *Pinelliae Rhizoma Praeparatum cum Zingibere* (Jiang Ban Xia), *Rhizoma Zingiberis Recens* (Sheng Jiang), *Radix asteris* (Zi Wan), *Flos farfarae* (Kuan Dong Hua), *Rhizoma Belamcandae* (She Gan), *Herba Asari* (Xi Xin), *Rhizoma Dioscoreae* (Shan Yao), *Fructus Aurantii Immaturus* (Zhi Shi), *Pericarpium Citri Reticulatae* (Chen Pi), and *Pogostemon Cablin (Blanco) Benth* (Guang Huo Xiang). Briefly, Sheng Shi Gao was decocted firstly, and then all raw materials were co-decocted in water twice (1 h for each time, the amount of the solvent was ten and eight times of the total weight of herbs, respectively). A total of approximate 1.78 L decoction were collected. The extracts were centrifuged at 10, 000 rpm for 20 min, and the supernatants were subject to LC–MS analysis.

2.3. LC-Q-TOF-MS analysis

An Acquity UPLC system (Waters, Milford, MA, USA) coupled with a Triple TOF 5600plus MS (AB SCIEX, Framingham, MA, USA), which equipped with an ESI source, was employed for chemical identification. Samples were separated on a Waters ACQUITY UPLC HSS T3 (150 mm × 2.1 mm i.d. 1.8 μm) at a flow rate of 0.3 mL/min and a column temperature of 50℃. Mobile phases A and B were 0.1 % formic acid-water and 0.1 % formic acid-acetonitrile, respectively. The linear gradient elution was optimized as follows: 0 − 2 min, 0 − 0%B; 2 − 25 min, 0–30 %B; 25 − 35 min, 30–95 %B; 35 − 37 min, 95 %B. The injection volume was 10 μL. The detection wave was 254 nm. Mass spectrometry analysis was performed in both positive and negative mode under following parameters: scan range, *m/z* 100–1500; ion source GS1 55 psi; ion source GS2, 55 psi; curation gas (CUR), 35 psi; temperature, 600℃ for ESI^+ and 550℃ for ESI^-; ionspray voltage (IS), −4.5 kV for ESI^- and 5.0 kV for ESI^+; declustering potential (DP), 100 V; collision energy (CE), 10 V.

2.4. Raw data-preprocessing parameters

The MS/MS data files were converted from the. wiff (Waters) standard data format to. mzXML format using the MSConvert software, within the ProteoWizard package. All. mzXML data were then processed using MZmine 2 v40.1 [22]. The mass detection was performed setting the noise level at 5.0 E4. The ADAP chromatogram builder was

used with a set of a minimum group size of scans of 5, a group intensity threshold of 100 000, a minimum highest intensity of 50 000 and a *m/z* tolerance of 0.001 Da (or 10 ppm) [23]. The ADAP wavelets deconvolution algorithm was used using S/N threshold = 10, minimum feature height = 5.0 E4, coefficient/area threshold = 100, peak duration range 0–1 min, RT wavelet range 0–0.2. MS/MS scans were paired using a *m/z* tolerance range of 0.02 Da and RT tolerance range of 0.1 min. Isotopic peaks grouper algorithm was used with an *m/z* tolerance of 0.001 Da (or 10 ppm) and an RT tolerance of 0.01 min. Peak alignment was performed using the join aligner module with *m/z* tolerance =0.001 Da (or 10 ppm), weight for *m/z* = 1, weight for RT = 1.0, absolute RT tolerance 0.1 min. The peak list was gap-filled with Peak finder module using *m/z* tolerance of 0.001 Da (or 10 ppm) and then filtered using Peak list row filter with retention time 0 − 42 min. Eventually, the mgf data file and its corresponding. csv metadata file including Peaks height and areas integration were exported.

2.5. Molecular networking

Corresponding molecular networking was created according to the online workflow at GNPS (http://gnps.ucsd.edu) with a parent mass tolerance of 0.02 Da and an MS/MS fragment ion tolerance of 0.02 Da, the minimum cluster size of 1, run MScluster and filter precursor window tools were turned off [24]. The network created with cosine score above 0.7 and more than four matched peaks. The spectra in the network were then searched against GNPS spectral libraries with a cosine score above 0.7 and at least 4 matched peaks. The molecular networking data were visualized using Cytoscape (ver.3.7.2).

2.6. Qingfei Paidu Decoction networking

After the compound network was created, potential therapeutic targets network for Qingfei Paidu Decoction were further established as previous studies [24–29]. First, we query and standardize the identified compound information by the Pubchem database [30]. As a result, all compounds were listed with CAS number or PubChem ID, which are for subsequent query work. Next, we collected the target points of each compound in the list through the ETCM [31] and SymMap databases [32]. At the same time, we searched the SMILE structure corresponding to each compound through the Pubchem database, entered the structure into the SWISS Target Prediction database [33] to predict possible targets, and collected targets with scores above 0.75 in the results. Finally , we used the DAVID database [34] to enrich the included target genes and visualized the enrichment results with Cytoscape (ver.3.7.2) and Power BI (ver. 2.79.5773.0).

2.7. COVID-19 disease network

At present, there are limited diagnostic indicators for COVID-19, and the variability in the detection process of the existing indicators directly leads to significant false negatives in the test. In comparison, the diagnostic system established according to the diagnosis of TCM mostly avoid false-negative results. Therefore, we established a COVID-19 disease network through the SymMap database according to the classification and symptoms from the TCM system in the 7th edition of *COVID-19 treatment guidelines*. First, we used the symptoms and their synonyms in the7th edition of *COVID-19 treatment guidelines* as search terms and entered them into SymMap. According to the symptom-drug-compound-target cycle, the database returns the target information corresponding to the symptoms. According to the classification of syndrome types in the 7th edition of *COVID-19 treatment guidelines*, we merged all collected targets and then performed enrichment analysis on targets through the DAVID database. After the enrichment analysis, we visualized the enriched results through the Enhancement Map and Annotation in Cytoscape (ver.3.7.2). Enrichment Map results only include those that contain more than 20 pathways or progresses.

2.8. The establishment of Qingfei Paidu Decoction therapeutic network for COVID-19

After getting the potential therapeutic targets of Qingfei Paidu Decoction and the target-genes of COVID-19, we further established the intervention network between Qingfei Paidu Decoction and COVID-19. In order to further focus the curative effect of Qingfei Paidu Decoction on the regulation of the immune system, especially in the regulation process of innate immunity, we mapped the drug-disease network of Qingfei Paidu Decoction and COVID-19 on the toll-like signaling pathway. Results were visualized with wikipathway plugin of Cytoscape software.

2.9. In vivo transcriptome experiment of Ma Xing Shi Gan Decoction

Male SD rats (110 ± 10 g, 8–9 weeks) were purchased from SPF (Beijing) Biotechnology Company. During housing, the animals were kept in standard polypropylene cages, and the room temperature and the humidity were maintained at 12/12-h light-dark cycle. Animals eat and drink freely.

After three days of adaptive breeding, the weight of all rats was measured. 50 SD rats were randomly divided into five groups, ten rats/group. The groups were named as normal group (Normal), model group (Model), Ma Xing Shi Gan Decoction (MXSG), antibiotic group (moxifloxacin), and hormone group (prednisone acetate). Next, the Model, MGXG, Antibiotic, and Hormone were received given 0.5 mg/mL LPS nebulization intervention, 30 min per day for three consecutive days. At the same time, on the day after the first atomization, the MGXG group, hormone group, and antibiotic group were given the oral treatment of Ma Xing Shi Gan Decoction, moxifloxacin, and prednisone acetate, which were administered orally once a day for three consecutive days. All doses were converted according to the equivalent dose of 0.018 for humans and rats with reference to clinical guidelines. After the last treatment, all the rats were on the condition of free drinking but without food for 12 h, then anesthetized with 10 % chloral hydrate and further sacrificed for liver, lung thymus, and kidney samples. The tissues were quickly collected, weighed, and the tissue/weight index was calculated and then placed in liquid nitrogen for quick freezing, and then placed in a − 80 °C refrigerator for later tests.

The total RNA from each of the different specimens was isolated from the lungs of rats of three groups (normal group, model group, and MXSG group) simultaneously using the RNeasy Mini-Kit (QIAGEN, Valencia, CA), as per the manufacturer's instructions. After extracting total RNA from the sample and digesting the DNA with DNase, enrich it with magnetic beads with Oligo (dT); then add a disruption reagent to break the mRNA into short fragments, use the disrupted mRNA as a template, and randomly use six bases. The primers are used to synthesize one-strand cDNA, and then a two-stranded reaction system is prepared to synthesize the two-stranded cDNA, and the double-stranded cDNA is purified; the purified double-stranded cDNA is then subjected to end repair, added with A tail, and connected to a sequencing adapter, and finally, PCR amplification is performed. After the library was qualified with the Agilent 2100 Bioanalyzer, it was sequenced using the Illumina HiSeqTM 2 sequencer to generate 125bp or 150bp double-ended data. After passing the quality inspection, sequencing was performed using an Illumina sequencer, and bioinformatics analysis were performed based on the results.

Gut microbiota of rats in different group were analyzed as previous study [35]. This study used a larger set of gut microbiota profiles that were generated alongside those described in a recent study by Goodrich et al. [36], which reported a smaller sample as it considered only complete twin pairs. The processing of fecal samples has been described previously [37]. Briefly, samples were collected by the individual at home and either bought to a clinical visit or posted on ice to the clinical research department on ice where it was stored at − 80 °C. Frozen samples were extracted to obtain DNA, the V4 region of the 16S rRNA

genes amplified, and amplicons sequenced using a multiplexed approach on the Illumina MiSeq platform. Sample reads were demultiplexed and paired-ends merged using a 200 nt minimum overlap.

De novo chimera removal was carried out on the 16S rRNA gene sequencing per sample using UCHIME [38]. Remaining reads were collapsed to de novo operational taxonomic units (OTUs) at 97 % identity using SUMACLUST within QIIME version 1.9.0 [39,40]. OTU taxonomy was assigned by aligning representative sequences to the Greengenes v13_8 database using UCLUST in QIIME. Analyses were adjusted for sequencing depth throughout by using sample read count as a covariate. Taxonomic abundances were generated by collapsing OTU counts at appropriate levels, followed by conversion to log-transformed relative abundances. Three alpha diversity metrics, namely the Shannon index, phylogenetic diversity, and raw OTU counts, were calculated using QIIME. Beta diversity was calculated as both weighted and unweighted UniFrac metrics, and principal coordinate analysis of the beta distances was carried out using the vegan package.

For histological evaluation, the formaldehyde-fixed lower lobe of the left lung was embedded in paraffin wax, serially sectioned, and stained with hematoxylin and eosin. Histologic changes, including alveolar wall edema, congestion, hemorrhage, and inflammatory cell infiltration, were evaluated under a light microscope to assess pulmonary inflammation according to the previous report [41].

2.10. Anti-inflammatory effect of glycyrrhizic acid in macrophage activation model

The RAW264.7 cell lines were cultured in high glucose DMEM with 10 % FBS and antibiotics (100 units/mL penicillin and 100 μg/mL streptomycin). The cells were seeded in 12-well plates at a density of 100,000 cells. After 1 day, the cells were co-incubated with LPS (100 ng/mL) or Poly(I:C) (10 μg/mL) + Pam3CSK4 (100 ng/mL) and test drug for 24 h. Dexamethasone acts as positive drug. After that, the cell culture medium was collected for IL-6 concentration measurement by enzyme-linked immunosorbent assay (ELISA) kit.

3. Results

3.1. Characterization of chemical constituents in Qingfei Paidu Decoction

Representative chromatograms obtained by UPLC-Q-TOF/MS are shown in Fig. 1. After analyzing the raw data, 151 peaks were caught as individual compounds. Among these, a total of 129 constituents were identified or tentatively characterized from QFPD based on literature and database matching. The compounds identified from QFPD were listed in Supplementary Table S1, including 58 flavonoids, 20 glycosides, 13 carboxylic acids, 7 saponins, 6 alkaloids, 4 terpenes, and other types of compounds. The main peaks in LC–MS chromatogram were labeled with chemical structures from different herbs (Supplementary Fig. S1). Among them, 29 compounds were unambiguously identified by comparisons with reference standards in terms of retention time and mass spectra (Supplementary Fig. S2). The number of chemical constituents of each herb and representative constituents chosen from identified list of QFPD was shown in Fig. 2, which suggested that GC, CH, HQ are the main sources of identified compounds.

MS/MS data were used to construct molecular networking of QFPD according to the classification of compound structures and its similarity in MS^2 spectra. As shown in Fig. 3, the colors of the nodes in the molecular networking represent the sources herb of the compounds, which clearly indicated the contribution of MH, GC, CH, SG, ZX to the chemical composition of QFPD. The sectorial area of color corresponding to the peak area of each compound. The size of nodes corresponds to the peak height of each compound in the whole decoction. Based on the networking, we labeled the represent compounds on the nodes, as shown in Fig. 4. Flavonoids aggregated to form the largest cluster, while glycosides and saponins also formed typical clusters.

3.2. Characterization of potential therapeutic targets of Qingfei Paidu Decoction

The potential therapeutic target-network of Qingfei Paidu Decoction was presented in Fig. 5. We firstly predicted and collected the targets of compounds identified by LC–MS. Qualified target information was obtained for 40 flavonoids, 7 glycosides, 5 terpenes, 3 carboxylic acids, 3 cholestanes, 2 saponins, 1 xanthenes, 1 heterocyclic, 1 benzopyrans, 1 benzofurans and 1 alkaloid. The links among the herbs, compound categories, and compounds were shown in Fig. 5A. Then, we counted the number of targets corresponding to each drug based on the compound information contained in the herbal medicine (Fig. 5B). The results showed that MH, GC, CH, HQ, ZW were the herbs with the highest number of corresponding targets. After merging all the target information and removing the duplicate target content, we next performed GO and KEGG enrichment analysis on the target information (Fig. 5C and D). As a result, in the GO enrichment analysis, QFPD played an interventional role by interfering with cellular processes and metabolic processes. The interventional effect was mainly on organelles and membrane structures, and the main targeted molecules were involved in protein binding process and the function of catalysis. KEGG analysis suggested that the effect of QFPD was mainly to interfere with viral infection-related pathways and cancer-related pathways. All the herb-compound-target information is in Supplementary Material 2.

3.3. The COVID-19 disease network

The construction of the COVID-19 symptom target network is based on TCM diagnostic system. According to the diagnostic criteria in the 7th edition of *COVID-19 treatment guidelines*, TCM classified COVID-19 patients into four categories based on patients' pathological process, including mild, moderate, severe, and critical. Among them, the mild type included the syndrome of cold fluid-retention suspend in lung and the syndrome of stagnant and jamming dampness-heat in the lung; the moderate type was divided into the syndrome of dampness toxin and depression of lung and the syndrome of accumulation of cold fluid in the lung; the severe type contained the syndrome of dirty-toxicity blocking lung and the syndrome of flaring heat in qifen (also known as defense qi, a term describes qi is "fierce, bold and uninhibited" and unable to contained by the vessels and therefore flowing out side them) and yingfen (also known as construction qi, which refer to the qi that forms the blood and flows with it in the vessels, helping to nourish the entire body) [42]; the critical type had only the syndrome of internal blockade and external collapse. We next collected the targets corresponding to the symptoms in the SymMap database according to the symptoms of different syndromes and the synonyms of the symptoms. The results showed that there were 1029 no-duplicate targets information in mild cases, of which the syndrome of cold fluid-retention suspend in lung contains 576 targets, whereas the syndrome of stagnant and jamming dampness-heat in lung contains 905 targets. For the moderate type, there were 638 targets for the syndrome of dampness toxin and depression of lung, and 611 targets for the syndrome of accumulation of cold fluid in the lung. For the severe type, 937 targets were collected for the syndrome of dirty-toxicity blocking lung, and 667 targets were collected for the syndrome of flaring heat in qifen and yingfen. Finally, for the critical type, 443 targets were included for the syndrome of the internal blockade and external collapse (Table 1).

We further analyzed these targets from COVID-19. The distribution of targets from different categories was shown in Fig. 6A. The results suggested that at different pathological stages (both class of mild, moderate, severe, and critical, or their divided categories), the targets that change during the pathological process are different. We then deduplicated, merged the target genes of the same class, and exhibited the results in the form of Venn diagrams (Fig. 6B). There are 233 targets in all four stages, and 376 targets appear in three stages, suggesting that in the pathological process of COVID-19, many biological processes may

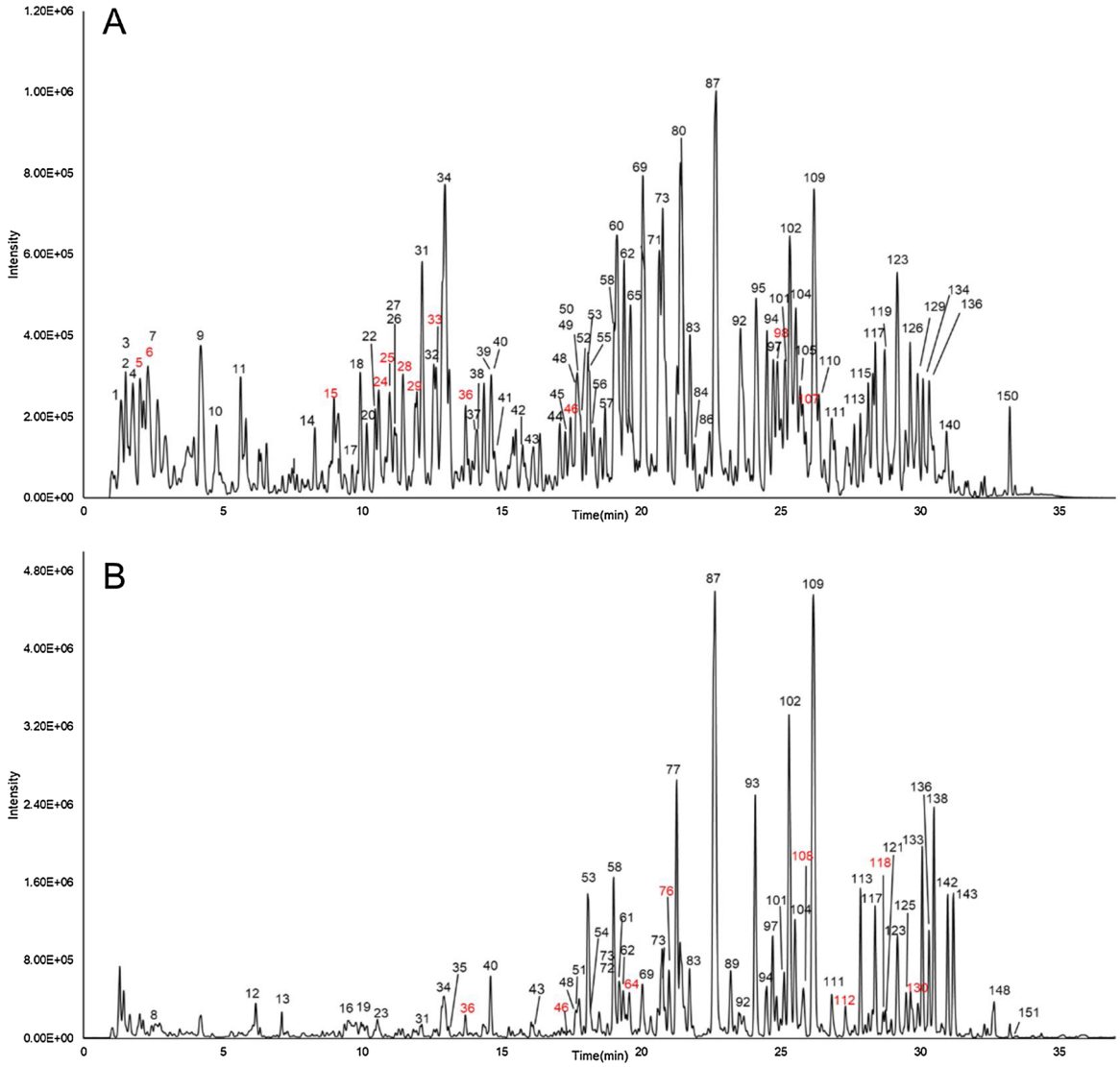

Fig. 1. Mass spectrum chromatograms of Qingfei Paidu Decoction (A) Negative mode (B) Positive mode. Red numbers represent unidentified compounds.

be shared (Supplementary Material 3). At the same time, in the transition phase, that is, mild phase to moderate phase, moderate phase to severe phase, severe phase to critical phase, the number of common targets appeared is relatively large, 77 between the mild and the moderate, 124 between the moderate and the severe, and between 82 the severe and the critical. To further find the regular of these targets, we merged, with no repetition, all the targets and then enriched these genes by GO and pathway (using the Reactome database) method. As a result, we found that targets were enriched in the regulation of a variety of biological processes and participated in the immune response process; the corresponding molecular functions of these genes were the docking, catalysis and molecular activity regulation of proteins; meanwhile, the positions of these targets correspond to subcellular organelles and cell membrane (Fig. 6C). This result was similar to the target network results of Qingfei Paidu Decoction, suggesting that Qingfei Paidu Decoction could be used as a promising formula to intervene in the pathological process of COVID-19. Moreover, we enriched the results of the biological process from GO and the results of pathways from Reactome database, and discover the immune regulation cells was the core physiological and pathological process of the pathological process of COVID-19 (Fig. 6D), which indicated that controlling the level of the immune response during the disease process was one of the crucial intervention to treating COVID-19.

3.4. The intervention of Qingfei Paidu Decoction for COVID-19 based on toll-like signaling pathway

As the Toll-like signaling pathway was one of the most critical pathways in the immune response to viral infections, we further investigate the effect of Qingfei Paidu Decoction for COVID-19 based on this pathway. We combined the potential therapeutic network of QFPD and the target network of COVID-19, and merged the result with the genes of the Toll-like signaling pathway. As a result, we found that a total of 24 genes are promising target genes of QFPD for COVID-19 (Fig. 7). Among the genes interfered by QFPD, 6 genes are reported as disease-related genes; 3 genes are target genes related to drug therapy, 12 genes are both disease-related genes and target genes, and 3 genes are background genes. When dissecting the compound-target relationships in the context of Toll-like receptor pathway, it is interesting to find out MH and GC, which belongs to Ma Xing Shi Gan Decoction, chiefly regulated the similar targets of QFPD.

3.5. Components variation of co-decoction of Ma Xing Shi Gan Decoction

Ma Xing Shi Gan Decoction, which consists of *Herba Ephedrae* (MH), *Semen armeniacae amarum* (Ku Xing Ren), *Gypsum fibrosum* (SSG) and *Radix Glycyrrhizae* (GC), was considered as the main efficacy part of the

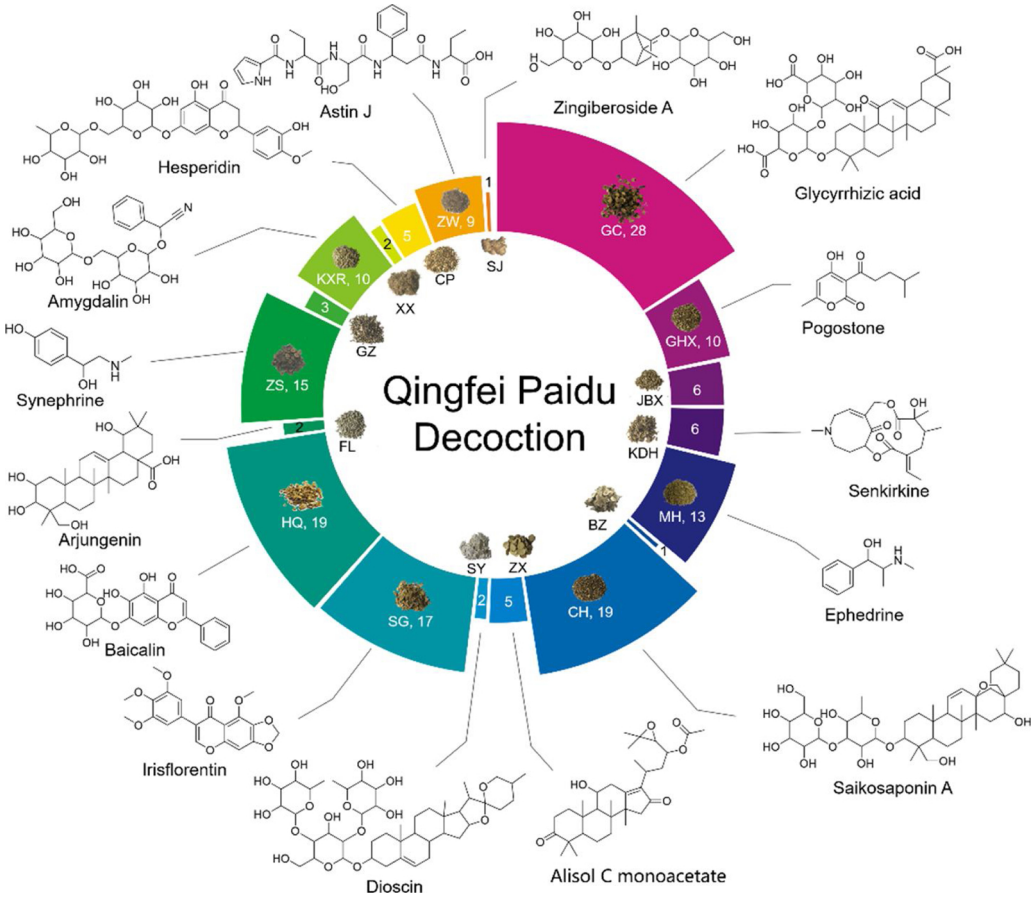

Fig. 2. The number of chemical constituents of each herbs and representative constituents structure identified from Qingfei Paidu Decoction.

whole decoction of QFPD. We also analyzed its chemical composition in parallel to the same LC–MS condition and investigated the synergistic effects on the content of main components, when different herbs were co-decocted and decocted individually (Fig. 8A). Based on the result of element analysis, it was found that the concentration of Manganese (Mn) and Nickel (Ni) arrived ppb level in the decoction after *Gypsum fibrosum* (SSG) was extracted for the first 30 min. It is interesting that the co-decoction of *Herba Ephedrae* (MH), *Gypsum fibrosum* (SSG), and *Radix Glycyrrhizae* (GC) lead to the increased yield rate of ephedrine (Fig. 8B). Conversely, the dissolution of glycyrrhizic acid was reduced during the co-decoction period, as shown in Fig. 8C, suggesting that the potential interaction between alkaloids (such as ephedrine) and glycyrrhizic acid may affects the chemical composition of Ma Xing Shi Gan Decoction.

3.6. The therapeutic effect of Ma Xing Shi Gan Decoction

We further validated the therapeutic effects of Ma Xing Shi Gan Decoction in a rat model of LPS induced pneumonia. Ma Xing Shi Gan Decoction significantly reduced the pulmonary inflammation response *in vivo* observed through pathological results (Supplementary Fig. S3A–E). The HE results showed that Ma Xing Shi Gan Decoction attenuated the LPS-induced inflammation in lung tissue.

The transcriptome of lung tissue results also showed that it was primarily related to complement and coagulation cascades, NOD-like receptor signaling pathway, antigen processing and presentation, cytosolic DNA-sensing pathway, RIG-I-like receptor signaling pathway, natural killer cell-mediated cytotoxicity, and IL-17 signaling pathway. These signaling pathways are closely related to the regulatory mechanism of the immune system (Supplementary Fig. S5). Vital proteins in these pathways, such as F12, F13b, F9, AT3, etc., were mainly concentrated in the blood coagulation system. These proteins were involved in the conversion of zymogen to serine protease, and eventually form thrombin, which is responsible for converting soluble fibrinogen into insoluble fibrin clot, affecting the regulation of innate immunity. The results suggested that the thrombin system might be one of the essential ways for Ma Xing Shi Gan Decoction to interfere with infection.

Besides, compared with the hormone and antibiotic groups, Ma Xing Shi Gan Decoction has higher safety. Safety evaluation based on HE staining, organ index, and intestinal flora were presented in Supplementary Fig. S4.

3.7. Glycyrrhizic acid attenuated the inflammatory response of macrophage

We further validated the anti-inflammatory effects of glycyrrhizic acid in cellular models of macrophage activation induced by different TLRs stimuluses. LPS stimulation is Toll-like receptor 4 (TLR4)-mediated response, while the combination of Poly(I:C) and Pam3CKS4 represents activation of TLR2 and TLR3. As shown in Fig. 9, both LPS or combination of Poly(I:C) and Pam3CKS4 stimulation significantly elevated the cytokine IL-6 levels in RAW264.7 cells. Glycyrrhizic acid (5 μM) significantly reduced the IL-6 release of macrophage after activation with both LPS (Fig. 9B) and Poly(I:C)/ Pam3CKS4 (Fig. 9C), suggesting that glycyrrhizic acid may exerts moderate anti-inflammatory effects through Toll-like receptor pathways

4. Discussion

COVID-19 has brought an enormous threat to human security. As of March 26, 2020, the number of deaths has been up to 24,065, which is about 3.4 % of the total confirmed cases [43]. In this present study, we

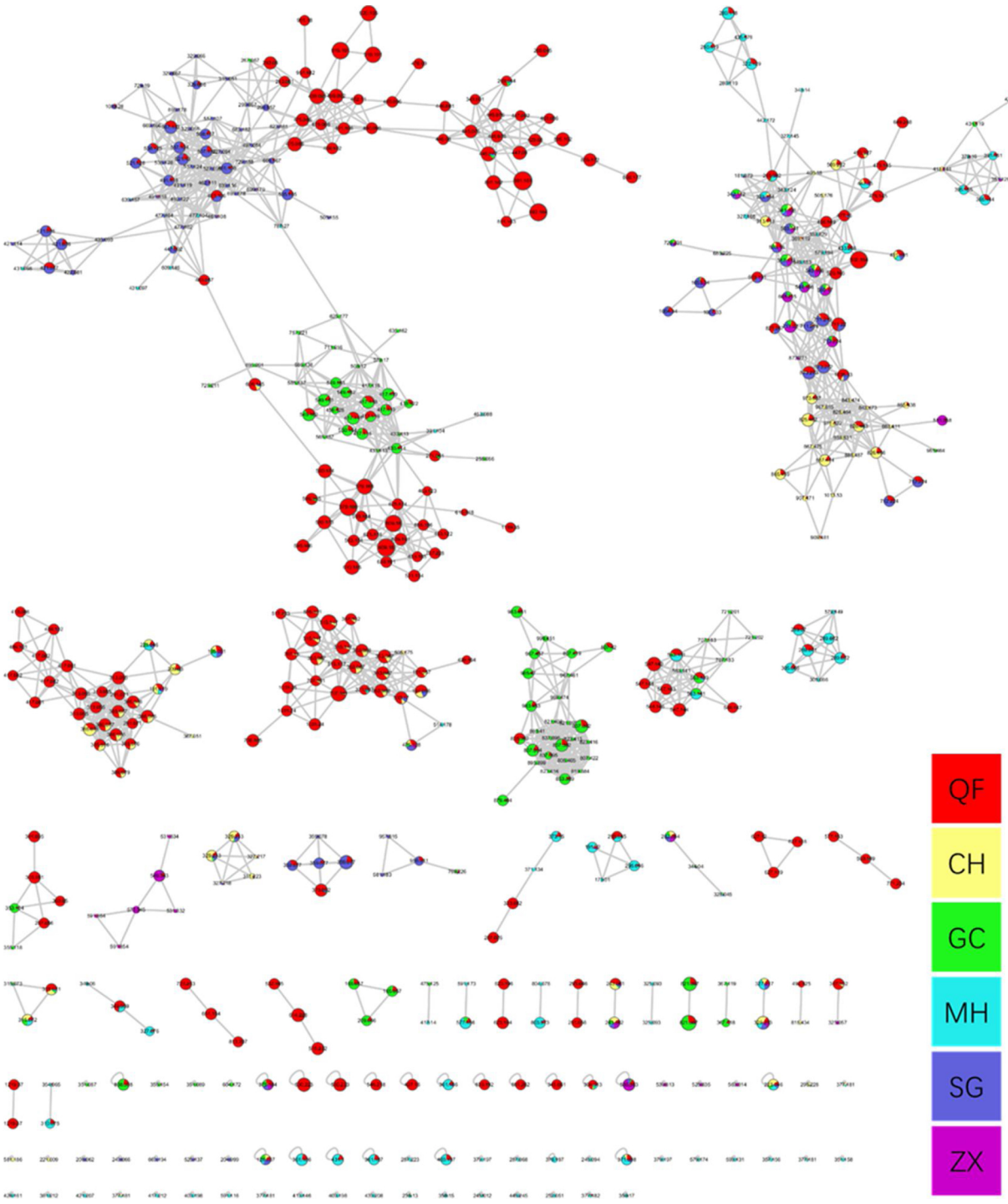

Fig. 3. Molecular networking of Qingfei Paidu Decoction.

construct a TCM symptom-target disease network of COVID-19 based on the diagnostic system of TCM, which is in 7th edition of *COVID-19 treatment guidelines* and has been used in the clinical treatment of COVID-19 in China. We found that in addition to the immune response and activation of multiple immune cells, the pathological processes of COVID-19 also involve in the coagulation system.

Using *in silico* approaches including network pharmacology and molecular networking of MS data, we elucidated the chemical composition and potential mechanism of QFPD against COVID-19. A total of 129 compounds were identified from QFPD, while the targets of these compounds in the context of COVID-19 disease network l were generated. As a result, we found that Toll-like signaling pathway plays important roles in pharmacological mechanism of QFPD for treating COVID-19. Compound from QFPD may directly interfere with Toll-like receptor 4 and regulate the downstream signaling pathways, including the NF-κB signaling pathway and MAPK signaling pathway, leading to the inhibition of release of proinflammation factors, such as TNF-α, IL-1β, IL-8. These cytokines may further induce the inflammation storm in COVID-19 [44], which is one of the most critical signs of the severe and critical condition of COVID-19, and the leading cause of patients death. Interestingly, based on the results of network pharmacology, QFPD may also regulate the downstream positions except for the Toll-like receptor 4, like PI3K, AKT, and CASP8, without interfering Toll-like receptor 2/3. Similarly, Qingfei Paidu Decoction also affects the INF-α response

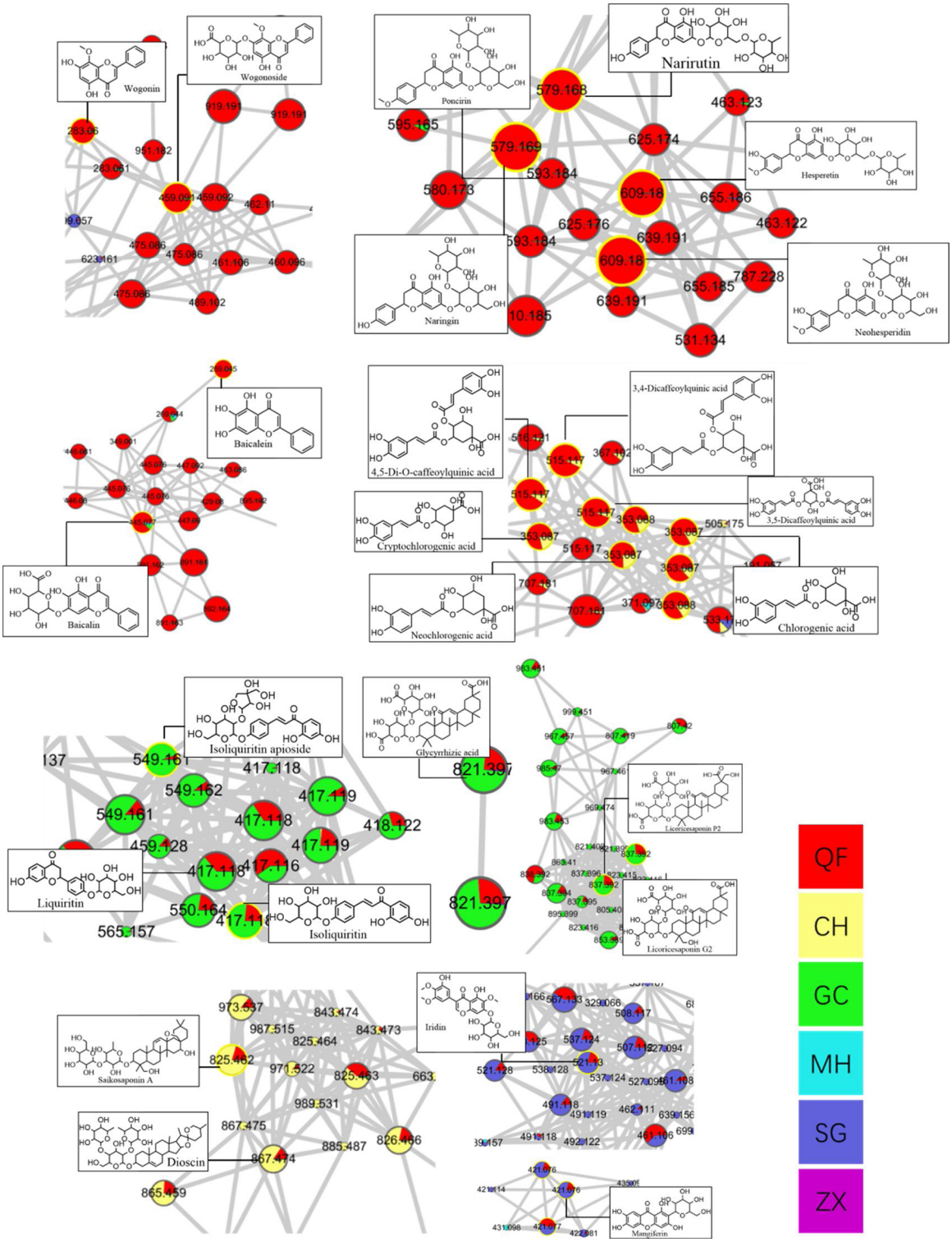

Fig. 4. Representative clusters of molecular networking of Qingfei Paidu Decoction.

induced by viral DNA or RNA invasion. These results indicate that QFPD may interfere with COVID-19 through multiple signaling pathways by multiple constituents from different TCMs.

As one of the components of QFPD, Ma Xing Shi Gan Decoction has been vastly used in the treatment of multiple epidemics caused by viruses [45–47]. Previous studies showed that Ma Xing Shi Gan Decoction can alleviate viral infection by regulating the expression of multiple cytokines, activating multiple innate immune-related cells, and preventing pathogens from entering targeted host cells [48–50]. In this present study, LC–MS results suggested that the compatibility of Ma Xing Shi Gan Decoction increase the dissolution of ephedrine while reducing the dissolution of glycyrrhizic acid. As one of the primary material foundations of Ma Xing Shi Gan Decoction, ephedrine has an anti-platelet aggregation effect [51]. Combined with the results of lung transcriptomics in this study, Ma Xing Shi Gan Decoction may enhance the effect of the whole prescription through intervention on the coagulation system.

Meanwhile, glycyrrhizic acid, an indispensable compound in the

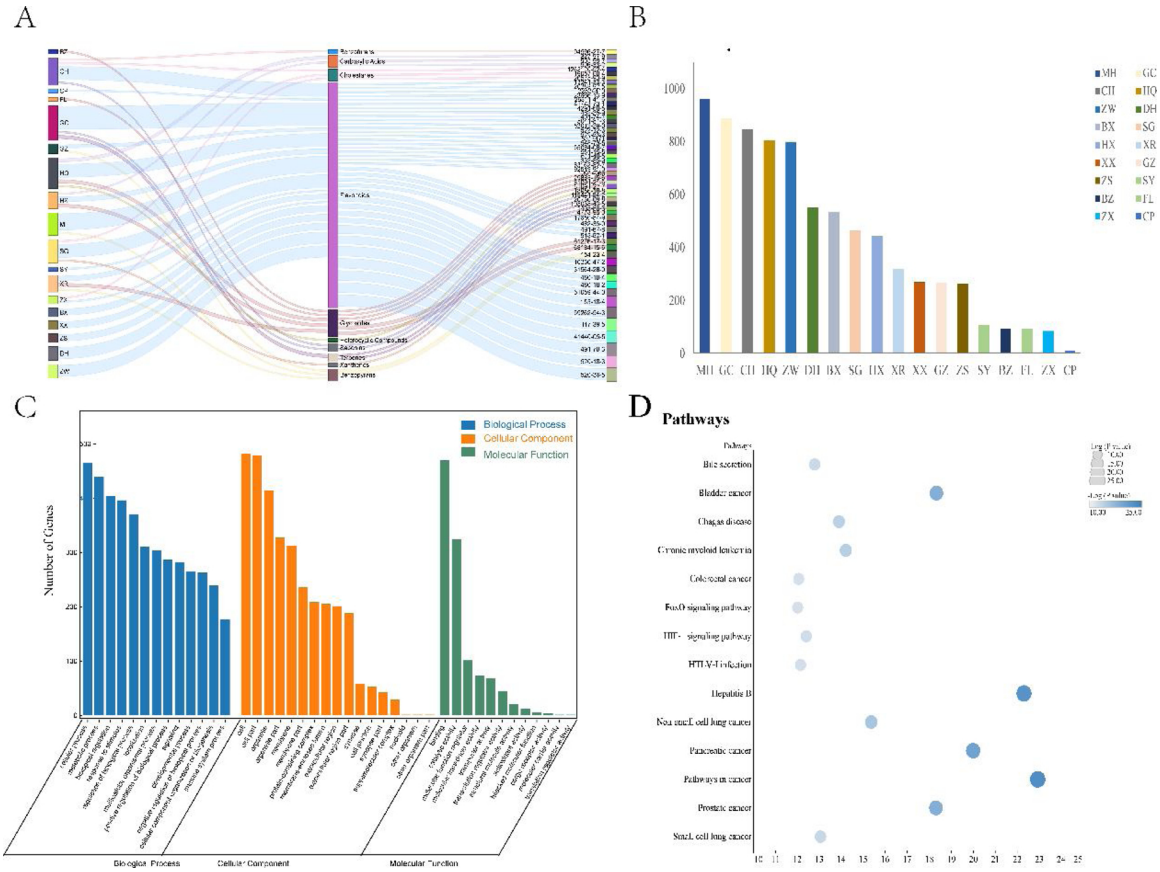

Fig. 5. The therapeutic network of Qingfei Paidu Decoction. (A) the distribution of compounds from different Chinese herbs. (B) the summary of potential targets genes from different herbs. (C) the GO enrichment of herbal-related genes. (D) the top 15 pathways enriched by the KEGG method. MH, *Herba Ephedrae* (Ma Huang); GC, *Radix Glycyrrhizae* (Gan Cao, baked); CH, *Stellariae Radix* (Chai Hu); HQ, *Radix Scutellariae* (Huang Qin); ZW, *Radix asteris* (Zi Wan); DH, *Flos farfarae* (Kuan Dong Hua); BX, *Pinelliae Rhizoma Praeparatum cum Zingibere* (Jiang Ban Xia); SG, *Rhizoma Belamcandae* (She Gan); *Pogostemon Cablin (Blanco) Benth* (Guang Huo Xiang); XR, *Semen armeniacae amarum* (Ku Xing Ren); XX, *Herba Asari* (Xi Xin); GZ, *Ramulus Cinmomi* (Gui Zhi); ZS, *Fructus Aurantii Immaturus* (Zhi Shi); SY, *Rhizoma Dioscoreae* (Shan Yao); BZ, *Atractylodis Macrocephalae Rhizoma* (Bai Zhu); FL, *Poria* (Fu Ling); ZX, *Rhizoma Alismatis* (Ze Xie); CP, *Pericarpium Citri Reticulatae* (Chen Pi).

whole recipe of Ma Xing Shi Gan Decoction, is a compound with a glucocorticoid-like effect [52]. Clinical data shown that glycyrrhizic acid has excellent anti-inflammatory, anti-oxidant and other suppressive immune response [53]. However, on the other hand, it may exerts side effects with potent cytotoxicity and bone damage characteristics [54]. This suggests that the therapeutic window of glycyrrhizic acid may be narrow. However, the co-decoction of Ma Xing Shi Gan Decoction lead to the controlled content of glycyrrhizic acid within a suitable dose range to exert anti-inflammatory effects without significant side effects. Due to limitation of time, whether glycyrrhizic acid

Table 1
The TCM symptoms of COVID-19 and potential therapeutic targets.

Class	Category	Symptoms	Gene number
Mild	Syndrome of cold fluid-retention suspend in lung	Fever, fatigue, sore body, cough, expectoration, chest tightness, shortness of breath, appetite, nausea, vomiting, and sticky stools. The tongue is pale, with creases or redness, the fur is white and thick, rotten or greasy, and the pulses are smooth or slippery	576
	Syndrome of stagnant and jamming dampness-heat in lung	Low or no fever, slight chills, fatigue, heavy head and body, muscle aches, dry sputum, sore throat, dry mouth, do not want to drink more or accompanied by chest tightness, no sweat or sweating, Nausea, diarrhea, or sticky stools. Reddish tongue, thick white or yellowish fur, slippery pulses	904
Moderate	Syndrome of dampness toxin and depression of lung	Fever, less cough, and sputum, or yellow sputum, tightness, shortness of breath, bloating, and constipation Dark red tongue, fat tongue, yellow greasy or yellow dry fur, slippery pulses or slippery strings	638
	Syndrome of accumulation of cold fluid in the lung	Low fever, no heat, or no heat, dry cough, less phlegm, fatigue, fatigue, chest tightness, nausea, or nausea. The tongue is pale or red, the fur is white or greasy, and the veins are floating and soft.	611
Severe	Syndrome of dirty-toxicity blocking lung	Fever redness, cough, yellowish phlegm stickiness, or blood in sputum, shortness of breath, shortness of breath, tiredness, dry mouth, and sticky mouth, nausea, poor stool, short urination. Red tongue, greasy yellow fur, slippery pulses	937
	Syndrome of flaring heat in qifen and yingfen	High fever and thirst, shortness of breath, shortness of breath, slang fainting, blurred vision, or spotted rash, or vomiting blood, bleeding, or convulsions in the limbs. Tongue ridges with little or no moss, fine pulse sinking or floating large	667
Critical	Syndrome of the internal blockade and external collapse	Dyspnea, dyspnea, or need mechanical ventilation, fainting, irritability, cold sweaty extremities, dark purple tongue, thick or dry fur, and floating pulses	443

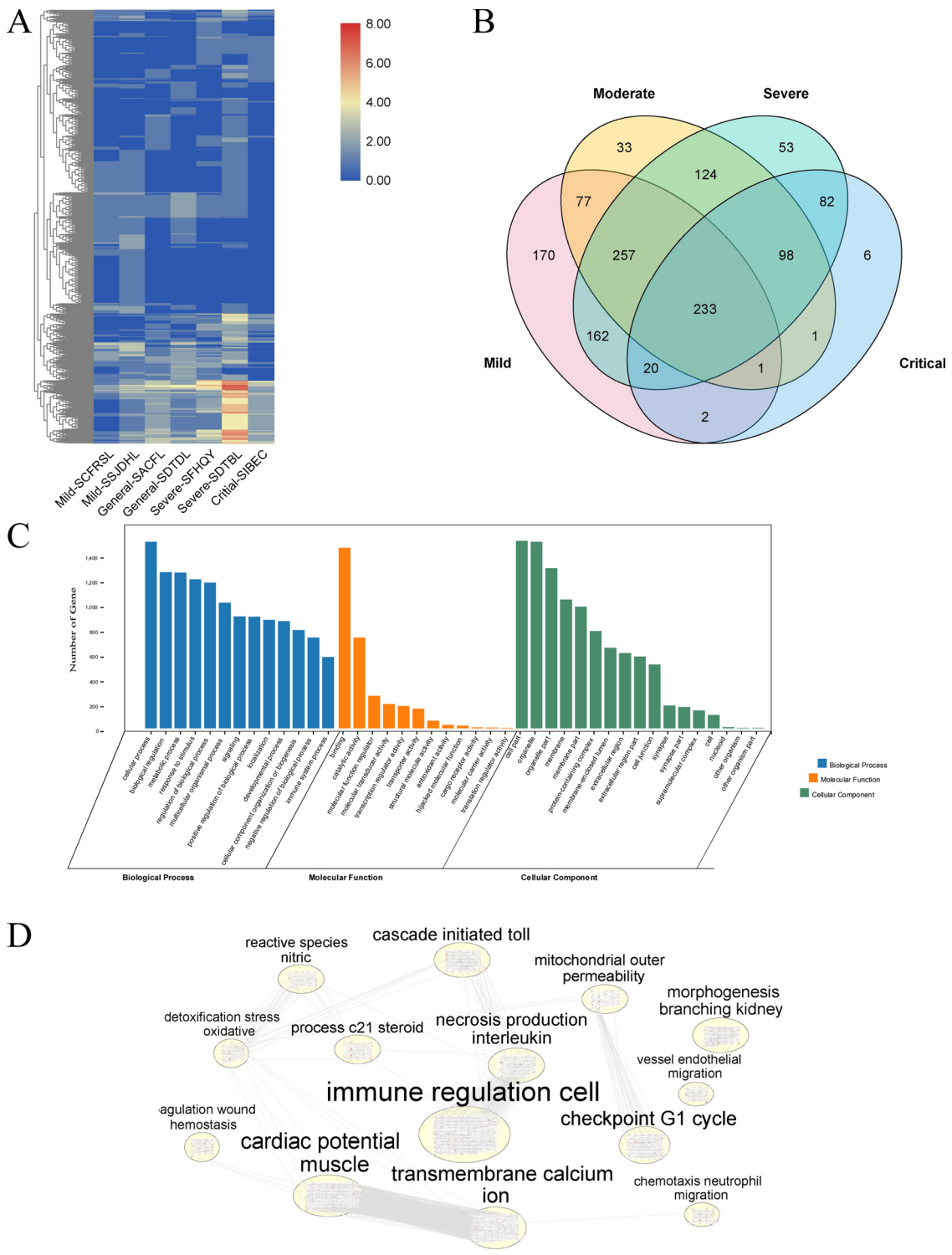

Fig. 6. The network of COVID-19. (A) the heatmap of different categories in diverse pathological classes based on TCM Diagnostic System. Each row refers to a target of COVID-19, while each column stand for a category of COVID-19 The color variety showed the frequency of the targets in each category. (B) Potential genes distribution of diverse pathological classes. (C) the enrichment of genes with GO method. (D) the enrichment of signaling pathways. SCFRSL, syndrome of cold fluid-retention suspend in the lung; SSJDHL, syndrome of stagnant and jamming dampness-heat in the lung; SACFL syndrome of dampness toxin and depression of lung; SDTDL, syndrome of accumulation of cold fluid in the lung; SFHQY, syndrome of dirty-toxicity bocking lung; SDTBL, syndrome of flaring heat in qifen and yingfen; SIBEC, syndrome of the internal blockade and external collapse.

and other major constituents of QFPD regulated other nodes and pathways in COVID-19 disease model are not fully investigated. Further research on the synergistic and additive effects of those compounds in QFPD will enhance our understanding on its pharmacological mechanism against COVID-19.

5. Conclusion

In this study, we illustrated the major chemical constituents as well as their potential targets of QFPD for treating COVID-19. By establishing a COVID-19 disease network and enriching the key nodes and

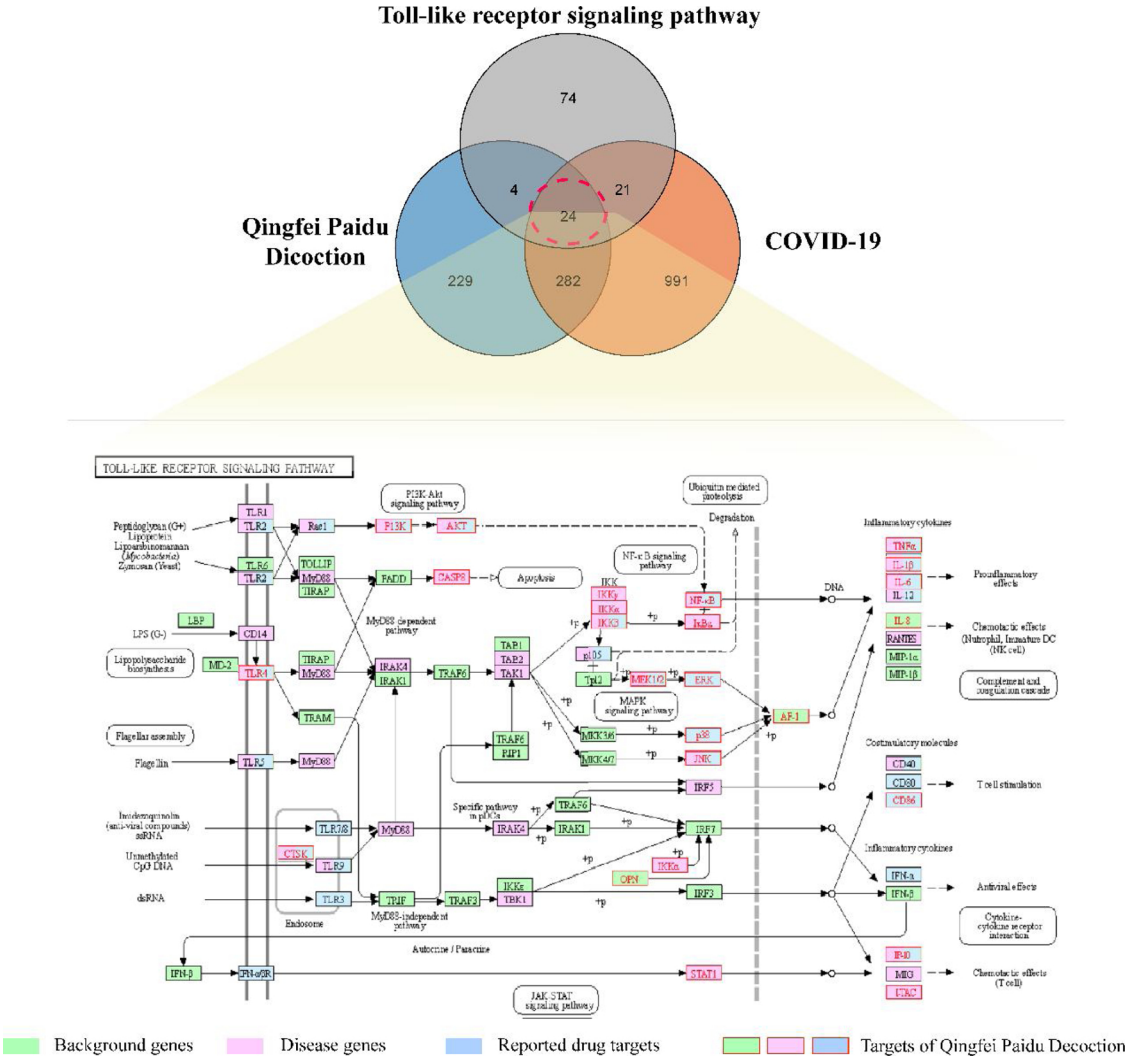

Fig. 7. The regulation of Qingfei Paidu Decoction on the Toll-like receptor signaling pathway.

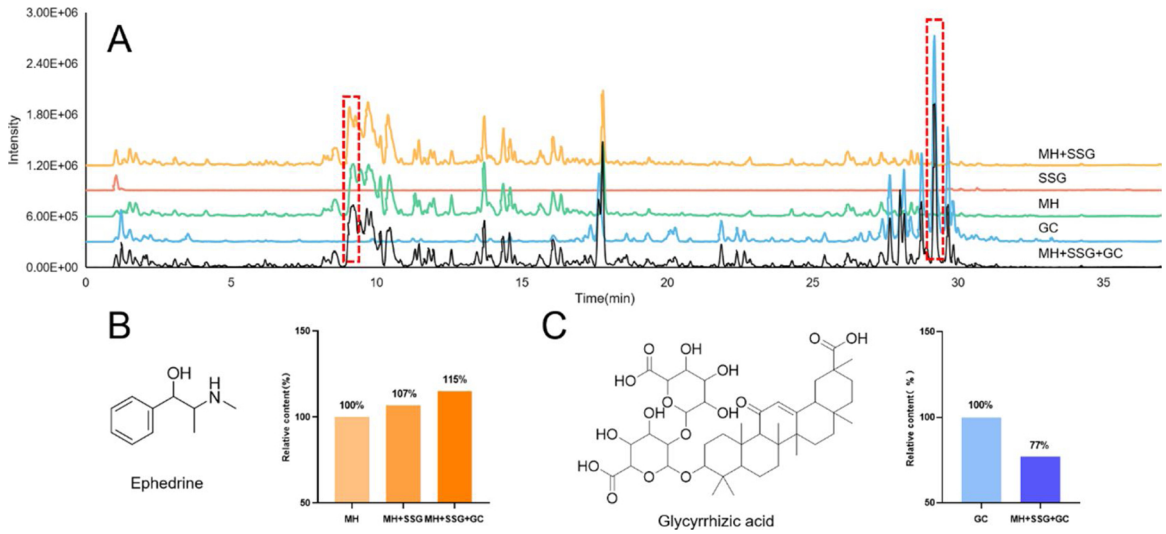

Fig. 8. The effects of components variation in Ma Xing Shi Gan Decoction on different decoction methods. (A) Comparison of mass spectrum chromatograms from four decoctions. (B) Effects of decoction methods on the relative content of ephedrine. (C) Effects of decoction methods on the relative content of glycyrrhizic acid.

pathways regulated by the active ingredients of QFPD, we found that Toll-like receptor signaling pathway play important role in pharmacological effects of QFPD. Interestingly, we found that Ma Xing Shi Gan Decoction, the core component of whole recipe may have a major contribution to the overall efficacy of QFPD. Further results of chemical analysis suggested that the contents of ephedrine and glycyrrhizic acid

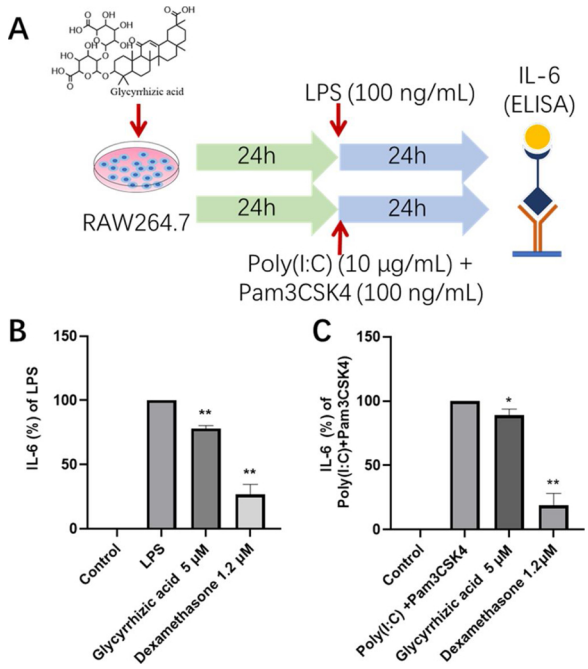

Fig. 9. Glycyrrhizic acid inhibits TLR agonists induced IL-6 production in RAW264.7. (A) Scheme of TLR agonists induced macrophage activation. Glycyrrhizic acid reduced the concentrations of IL-6 released by macrophage activated by LPS (B) or Poly(I:C)/ Pam3CKS4 (C), compared with LPS or Poly (I:C)/Pam3CKS4, $*P < 0.05$, $**P < 0.01$.

changed after decoction. Transcriptomic analysis of effects of Ma Xing Shi Gan Decoction in a rat model of pneumonia suggested that it regulated the coagulation system in the inflammatory state, which benefits QFPD to intervene the inflammatory storm caused by COVID-19. Our research provides an experimental and computational basis and research ideas for further discovery of TCM formula and botanical drug for the treatment of COVID-19.

Declaration of Competing Interest

The authors declare there are no known conflicts of interest associated with this publication and there has been no significant financial support for this work that could have influenced its outcome.

Acknowledgements

This work was supported by the National Natural Science Foundation of China (No. 81822047), Double First-Class Personnel Office-High Level Scientific Research Team Research Fund (1000061020100), National Key R&D Program of China (2017YFC1700106), Fundamental Research Funds for the Central Universities (2019-JYB-JS-007, 2019-JYB-XS-004), China Postdoctoral Science Foundation (2019M650593).

Appendix A. Supplementary data

Supplementary material related to this article can be found, in the online version, at doi:https://doi.org/10.1016/j.phrs.2020.104820.

References

[1] C. Wang, P.W. Horby, F.G. Hayden, G.F. Gao, A novel coronavirus outbreak of global health concern, Lancet 395 (10223) (2020) 470–473.
[2] N. Chen, M. Zhou, X. Dong, J. Qu, F. Gong, Y. Han, Y. Qiu, J. Wang, Y. Liu, Y. Wei, J.a. Xia, T. Yu, X. Zhang, L. Zhang, Epidemiological and clinical characteristics of 99 cases of 2019 novel coronavirus pneumonia in Wuhan, China: a descriptive study, Lancet (London, England) 395 (10223) (2020) 507–513.
[3] Q. Li, X. Guan, P. Wu, X. Wang, L. Zhou, Y. Tong, R. Ren, K.S.M. Leung, E.H.Y. Lau, J.Y. Wong, X. Xing, N. Xiang, Y. Wu, C. Li, Q. Chen, D. Li, T. Liu, J. Zhao, M. Li, W. Tu, C. Chen, L. Jin, R. Yang, Q. Wang, S. Zhou, R. Wang, H. Liu, Y. Luo, Y. Liu, G. Shao, H. Li, Z. Tao, Y. Yang, Z. Deng, B. Liu, Z. Ma, Y. Zhang, G. Shi, T.T.Y. Lam, J.T.K. Wu, G.F. Gao, B.J. Cowling, B. Yang, G.M. Leung, Z. Feng, Early transmission dynamics in Wuhan, China, of novel coronavirus-infected pneumonia, N. Engl. J. Med. (2020).
[4] Coronavirus COVID-19 Global Cases by Johns Hopkins CSSE. www.gisanddata.maps.arcgis.com.
[5] 2019–20 coronavirus outbreak. https://en.wikipedia.org/wiki/2019%E2%80%9320_coronavirus_outbreak#cite_note-JHMap-3.
[6] W.-J. Guan, Z.-Y. Ni, Y. Hu, W.-H. Liang, C.-Q. Ou, J.-X. He, et al., Characteristics of coronavirus disease 2019 in China, N. Engl. J. Med. (2020).
[7] J.R. Tisoncik, M.J. Korth, C.P. Simmons, J. Farrar, T.R. Martin, M.G. Katze, Into the eye of the cytokine storm, Microbiol. Mol. Biol. Rev. 76 (1) (2012) 16–32.
[8] B.G. Chousterman, F.K. Swirski, G.F. Weber, Cytokine storm and sepsis disease pathogenesis, Semin. Immunopathol. 39 (5) (2017) 517–528.
[9] Off-label use of medicines for COVID-19. https://www.who.int/news-room/commentaries/detail/off-label-use-of-medicines-for-covid-19.
[10] WHO launches global megatrial of the four most promising coronavirus treatments. https://www.sciencemag.org/news/2020/03/who-launches-global-megatrial-four-most-promising-coronavirus-treatments.
[11] K. Xu, H. Cai, S. Yihong, N. Qin, C. Yu, H. Shaohua, L. Jianping, W. Huafen, Y. Liang, H. He, Q. Yunqing, W. Guoqing, F. Qiang, Z. Jianying, S. Jifang, L. Tingbo, L. Lanjuan, Management of corona virus disease-19 (COVID-19): the Zhejiang experience, J. Zhejiang Univ. (Medical Sciences) (2020) 1–12.
[12] R.S. Hardy, H. Zhou, M.J. Seibel, M.S. Cooper, Glucocorticoids and bone: consequences of endogenous and exogenous excess and replacement therapy, Endocr. Rev. 39 (5) (2018) 519–548.
[13] M. Oray, K. Abu Samra, N. Ebrahimiadib, H. Meese, C.S. Foster, Long-term side effects of glucocorticoids, Expert Opin. Drug Saf. 15 (4) (2016) 457–465.
[14] Beijing: The total effective rate of traditional Chinese medicine treatment of new crown pneumonia is 92%. http://www.xinhuanet.com/local/2020-02/24/c_1125620808.htm.
[15] Established Xinguan Rehabilitation Clinic, TCM participated in the whole process of treatment. http://www.satcm.gov.cn/xinxifabu/meitibaodao/2020-03-04/13603.html.
[16] J.-L. Ren, A.-H. Zhang, X.-J. Wang, Traditional Chinese medicine for COVID-19 treatment, Pharmacol. Res. 155 (2020) 104743.
[17] Notice on Printing and Distributing Pneumonia Diagnosis and Treatment Plan for New Coronavirus Infection (Trial Version). http://www.nhc.gov.cn/xcs/zhengcwj/202001/f492c9153ea9437bb587ce2ffcbee1fa.shtml.
[18] Notice regarding the issuance of a new coronavirus pneumonia diagnosis and treatment plan (for trial version 6). http://www.gov.cn/zhengce/zhengceku/2020-02/19/content_5480948.htm.
[19] L. Chen, J. Xie, Interpretation of "New Coronavirus Pneumonia Diagnosis and Treatment Program (Trial Version 7)", Herald Med. (Herald Med) (2020) 1–6.
[20] N.H.C.o.t. PRC, S.A.o.T.C. Medicine, 6th edition of COVID-19 treatment guidelines Chinese Journal of Viral Diseases 1–5.
[21] W. Raoqiong, Y. Sijin, X. Chunguang, S. Qilin, L. Minqing, L. Xiao, L. Jike, H. Mei, Clinical observation of Qingfei Paidu Decoction in treating COVID-19, Pharmacol. Clin. Chin. Materia Med. (2020) 1–14.
[22] T. Pluskal, S. Castillo, A. Villar-Briones, M. Oresic, MZmine 2: modular framework for processing, visualizing, and analyzing mass spectrometry-based molecular profile data, BMC Bioinf. 11 (2010) 395.
[23] X. Du, A. Smirnov, T. Pluskal, W. Jia, S. Sumner, Metabolomics data preprocessing using ADAP and MZmine 2, Methods Mol. Biol. 2104 (2020) 25–48.
[24] M. Wang, J.J. Carver, V.V. Phelan, L.M. Sanchez, N. Garg, Y. Peng, D.D. Nguyen, J. Watrous, C.A. Kapono, T. Luzzatto-Knaan, C. Porto, A. Bouslimani, A.V. Melnik, M.J. Meehan, W.T. Liu, M. Crusemann, P.D. Boudreau, E. Esquenazi, M. Sandoval-Calderon, R.D. Kersten, L.A. Pace, R.A. Quinn, K.R. Duncan, C.C. Hsu, D.J. Floros, R.G. Gavilan, K. Kleigrewe, T. Northen, R.J. Dutton, D. Parrot, E.E. Carlson, B. Aigle, C.F. Michelsen, L. Jelsbak, C. Sohlenkamp, P. Pevzner, A. Edlund, J. McLean, J. Piel, B.T. Murphy, L. Gerwick, C.C. Liaw, Y.L. Yang, H.U. Humpf, M. Maansson, R.A. Keyzers, A.C. Sims, A.R. Johnson, A.M. Sidebottom, B.E. Sedio, A. Klitgaard, CABP, D. Torres-Mendoza, D.J. Gonzalez, D.B. Silva, L.M. Marques, D.P. Demarque, E. Pociute, E.C. O'Neill, E. Briand, E.J.N. Helfrich, E.A. Granatosky, E. Glukhov, F. Ryffel, H. Houson, H. Mohimani, J.J. Kharbush, Y. Zeng, J.A. Vorholt, K.L. Kurita, P. Charusanti, K.L. McPhail, K.F. Nielsen, L. Vuong, M. Elfeki, M.F. Traxler, N. Engene, N. Koyama, O.B. Vining, R. Baric, R.R. Silva, S.J. Mascuch, S. Tomasi, S. Jenkins, V. Macherla, T. Hoffman, V. Agarwal, P.G. Williams, J. Dai, R. Neupane, J. Gurr, A.M.C. Rodriguez, A. Lamsa, C. Zhang, K. Dorrestein, B.M. Duggan, J. Almaliti, P.M. Allard, P. Phapale, L.F. Nothias, T. Alexandrov, M. Litaudon, J.L. Wolfender, J.E. Kyle, T.O. Metz, T. Peryea, D.T. Nguyen, D. VanLeer, P. Shinn, A. Jadhav, R. Muller, K.M. Waters, W. Shi, X. Liu, L. Zhang, R. Knight, P.R. Jensen, B.O. Palsson, K. Pogliano, R.G. Linington, M. Gutierrez, N.P. Lopes, W.H. Gerwick, B.S. Moore, P.C. Dorrestein, N. Bandeira, Sharing and community curation of mass spectrometry data with Global Natural Products Social Molecular Networking, Nat. Biotechnol. 34 (8) (2016) 828–837.
[25] K. Gao, R. Yang, J. Zhang, Z. Wang, C. Jia, F. Zhang, S. Li, J. Wang, G. Murtaza, H. Xie, H. Zhao, W. Wang, J. Chen, Effects of Qijian mixture on type 2 diabetes assessed by metabonomics, gut microbiota and network pharmacology, Pharmacol. Res. 130 (2018).
[26] P. Li, J. Chen, W. Zhang, H. Li, W. Wang, J. Chen, Network pharmacology based investigation of the effects of herbal ingredients on the immune dysfunction in heart

disease, Pharmacol. Res. 141 (2019) 104–113.
[27] H. Lu, J. Zhang, Y. Liang, Y. Qiao, C. Yang, X. He, W. Wang, S. Zhao, D. Wei, H. Li, W. Cheng, Z. Zhang, Network topology and machine learning analyses reveal microstructural white matter changes underlying Chinese medicine Dengzhan Shengmai treatment on patients with vascular cognitive impairment, Pharmacol. Res. 156 (2020) 104773.
[28] G. Tian, C. Wu, J. Li, B. Liang, F. Zhang, X. Fan, Z. Li, Y. Wang, Z. Li, D. Liu, E. Lai-Han Leung, J. Chen, Network pharmacology based investigation into the effect and mechanism of Modified Sijunzi Decoction against the subtypes of chronic atrophic gastritis, Pharmacol. Res. 144 (2019) 158–166.
[29] X. Xu, C. Zhang, P. Li, F. Zhang, K. Gao, J. Chen, H. Shang, Drug-symptom networking: linking drug-likeness screening to drug discovery, Pharmacol. Res. 103 (2016) 105–113.
[30] S. Kim, J. Chen, T. Cheng, A. Gindulyte, J. He, S. He, Q. Li, B.A. Shoemaker, P.A. Thiessen, B. Yu, L. Zaslavsky, J. Zhang, E.E. Bolton, PubChem 2019 update: improved access to chemical data, Nucleic Acids Res. 47 (D1) (2019) D1102–D1109.
[31] H.-Y. Xu, Y.-Q. Zhang, Z.-M. Liu, T. Chen, C.-Y. Lv, S.-H. Tang, X.-B. Zhang, W. Zhang, Z.-Y. Li, R.-R. Zhou, H.-J. Yang, X.-J. Wang, L.-Q. Huang, ETCM: an encyclopaedia of traditional Chinese medicine, Nucleic Acids Res. 47 (D1) (2019) D976–D982.
[32] Y. Wu, F. Zhang, K. Yang, S. Fang, D. Bu, H. Li, L. Sun, H. Hu, K. Gao, W. Wang, X. Zhou, Y. Zhao, J. Chen, SymMap: an integrative database of traditional Chinese medicine enhanced by symptom mapping, Nucleic Acids Res. 47 (D1) (2019) D1110–D1117.
[33] D. Gfeller, A. Grosdidier, M. Wirth, A. Daina, O. Michielin, V. Zoete, SwissTargetPrediction: a web server for target prediction of bioactive small molecules, Nucleic Acids Res. 42 (Web Server issue) (2014) W32–W38.
[34] G. Dennis, B.T. Sherman, D.A. Hosack, J. Yang, W. Gao, H.C. Lane, R.A. Lempicki, DAVID: database for annotation, visualization, and integrated discovery, Genome Biol. 4 (5) (2003) P3.
[35] M.A. Jackson, S. Verdi, M.-E. Maxan, C.M. Shin, J. Zierer, R.C.E. Bowyer, T. Martin, F.M.K. Williams, C. Menni, J.T. Bell, T.D. Spector, C.J. Steves, Gut microbiota associations with common diseases and prescription medications in a population-based cohort, Nat. Commun. 9 (1) (2018) 2655.
[36] J.K. Goodrich, E.R. Davenport, M. Beaumont, M.A. Jackson, R. Knight, C. Ober, T.D. Spector, J.T. Bell, A.G. Clark, R.E. Ley, Genetic determinants of the gut microbiome in UK Twins, Cell Host Microbe 19 (5) (2016) 731–743.
[37] J.K. Goodrich, J.L. Waters, A.C. Poole, J.L. Sutter, O. Koren, R. Blekhman, M. Beaumont, W. Van Treuren, R. Knight, J.T. Bell, T.D. Spector, A.G. Clark, R.E. Ley, Human genetics shape the gut microbiome, Cell 159 (4) (2014) 789–799.
[38] R.C. Edgar, B.J. Haas, J.C. Clemente, C. Quince, R. Knight, UCHIME improves sensitivity and speed of chimera detection, Bioinformatics 27 (16) (2011) 2194–2200.
[39] J.G. Caporaso, J. Kuczynski, J. Stombaugh, K. Bittinger, F.D. Bushman, E.K. Costello, N. Fierer, A.G. Peña, J.K. Goodrich, J.I. Gordon, G.A. Huttley, S.T. Kelley, D. Knights, J.E. Koenig, R.E. Ley, C.A. Lozupone, D. McDonald, B.D. Muegge, M. Pirrung, J. Reeder, J.R. Sevinsky, P.J. Turnbaugh, W.A. Walters, J. Widmann, T. Yatsunenko, J. Zaneveld, R. Knight, QIIME allows analysis of high-throughput community sequencing data, Nat. Methods 7 (5) (2010) 335–336.
[40] M.A. Jackson, J.T. Bell, T.D. Spector, C.J. Steves, A heritability-based comparison of methods used to cluster 16S rRNA gene sequences into operational taxonomic units, PeerJ 4 (2016) e2341.
[41] C.H. Yang, P.S. Tsai, T.-Y. Wang, C.J. Huang, Dexmedetomidine-ketamine combination mitigates acute lung injury in haemorrhagic shock rats, Resuscitation (2009) (1873-1570(Electronic)).
[42] F.Y. Nigel Wiseman, Introduction to English Terminology of Chinese Medicine, Paradigm Pubns; Bilingual edition, Brookline, Massachusetts, 2002.
[43] Coronavirus (COVID-19) Mortality Rate. www.worldometers.info.
[44] P. Mehta, D.F. McAuley, M. Brown, E. Sanchez, R.S. Tattersall, J.J. Manson, COVID-19: consider cytokine storm syndromes and immunosuppression, Lancet (London, England) (2020).
[45] J. Ding, Z. Qinyu, C. Xinmin, H. Jing, Implications of SARS TCM diagnosis and treatment in Beijing and Guangdong: 13 years of SARS, Lishizhen Med. Materia Med. Res. 28 (5) (2017) 1167–1169.
[46] C. Wang, B. Cao, Q.-Q. Li, Z.-Q. Zou, Z.-A. Li, L. Gu, et al., Oseltamivir compared with the Chinese traditional therapy Maxingshigan-Yinqiaosan in the treatment of H1N1 influenza: a randomized trial, Ann. Intern. Med. 155 (4) (2011) 217–225.
[47] Z. Yilan, L. Dafeng, L. Yaling, C. Hong, B. Yun, W. Xianmin, Z. Xiaofei, W. Wei, A randomized controlled study of maxing Shigan Decoction in the treatment of mild H1N1 influenza, Modern Prev. Med. 38 (12) (2011) 2227-2230 + 2239.
[48] Y.-X. Fei, B. Zhao, Q.-Y. Yin, Y.-Y. Qiu, G.-H. Ren, B.-W. Wang, Y.-F. Wang, W.-R. Fang, Y.-M. Li, Ma Xing Shi Gan Decoction attenuates PM2.5 induced lung injury via inhibiting HMGB1/TLR4/NFκB signal pathway in rat, Front. Pharmacol. 10 (2019) 1361.
[49] C.-F. Hsieh, C.-W. Lo, C.-H. Liu, S. Lin, H.-R. Yen, T.-Y. Lin, J.-T. Horng, Mechanism by which Ma-Xing-Shi-Gan-Tang inhibits the entry of influenza virus, J. Ethnopharmacol. 143 (1) (2012) 57–67.
[50] S.T. Kao, T.J. Yeh, C.C. Hsieh, H.B. Shiau, F.T. Yeh, J.G. Lin, The effects of Ma-Xing-Gan-Shi-Tang on respiratory resistance and airway leukocyte infiltration in asthmatic guinea pigs, Immunopharmacol. Immunotoxicol. 23 (3) (2001) 445–458.
[51] P.A. Flordal, J. Svensson, Hemostatic effects of ephedrine, Thromb. Res. 68 (3) (1992) 295–302.
[52] T.-C. Kao, M.-H. Shyu, G.-C. Yen, Glycyrrhizic acid and 18beta-glycyrrhetinic acid inhibit inflammation via PI3K/Akt/GSK3beta signaling and glucocorticoid receptor activation, J. Agric. Food Chem. 58 (15) (2010) 8623–8629.
[53] X. Li, R. Sun, R. Liu, Natural products in licorice for the therapy of liver diseases: progress and future opportunities, Pharmacol. Res. 144 (2019) 210–226.
[54] S. Nazari, M. Rameshrad, H. Hosseinzadeh, Toxicological effects of Glycyrrhiza glabra (Licorice): a review, Phytother. Res. 31 (11) (2017) 1635–1650.